

# Optimizing B-spline surfaces for developability and paneling architectural freeform surfaces

K. Gavril<sup>a,b</sup>, A. Schiftner<sup>b</sup>, H. Pottmann<sup>a</sup>

<sup>a</sup>*Applied Geometry, Institute of Discrete Mathematics and Geometry,  
Vienna University of Technology, Wiedner Hauptstrasse 8-10/104, A-1040 Vienna, Austria*  
<sup>b</sup>*Evolute GmbH, Schwindgasse 4/10, 1040 Vienna, Austria*

---

## Abstract

Motivated by applications in architecture and design, we present a novel method for increasing the developability of a B-spline surface. We use the property that the Gauss image of a developable surface is 1-dimensional and can be locally well approximated by circles. This is cast into an algorithm for thinning the Gauss image by increasing the planarity of the Gauss images of appropriate neighborhoods. A variation of the main method allows us to tackle the problem of paneling a freeform architectural surface with developable panels, in particular enforcing rotational cylindrical, rotational conical and planar panels, which are the main preferred types of developable panels in architecture due to the reduced cost of manufacturing.

*Keywords:* developable surface, spline surface, architectural geometry, computational differential geometry, constrained optimization

---

## 1. Introduction

Developable surfaces can be locally mapped to a planar domain without distortion. Since they can be constructed from an initial planar state without stretching or tearing, only by bending, they represent the shapes obtainable with thin materials like sheet metal or paper which do not stretch. These surfaces are of great interest to many applications. Areas like architecture, manufacturing and design take advantage of the cost-reduced manufacturing process that developables have.

Developable surfaces have been well studied in classical differential geometry. Developable, twice differentiable surfaces are *single curved*, meaning one of the principal curvatures is zero. Thus, the Gauss curvature vanishes at every point. They are composed of special *ruled* surfaces with a constant tangent plane at all points of a ruling. As the surface normal vectors along a ruling agree, the Gauss image of a developable surface is 1-dimensional, i.e. a curve.

We base the main method in our paper on this property of the Gauss image. However, our focus is not on exact developability, but rather on *nearly developable* surfaces which we characterize by nearly curve-like Gauss images. The motivation for our research is the fact that most materials allow for a little bit of stretching and therefore developability needs not be satisfied to a high degree in a variety of applications. In particular, we are interested in applications in architecture where various kinds of tolerances can be exploited to reduce the production cost of freeform skins. Our work fits into a larger research program on novel digital tools which consider key aspects of function and fabrication, including material behavior, already in the early design and digital modeling phase.

**Previous work.** There is a vast amount of literature on developable surfaces, on their theory, their computational design using various types of representations and on their appearance in numerous applications. We limit this discussion to three main areas which are most closely related to our work: (i) developable Bezier and B-spline surfaces, (ii) discrete representations and nearly developable surfaces and (iii) their importance in paneling architectural surfaces.

*Developable Bezier and B-spline surfaces.* Lang and Röschel [1] expressed developability of rational, in particular polynomial Bézier surfaces in a system of cubic equations. In general, this

---

*Email addresses:* [gavril@evolute.at](mailto:gavril@evolute.at) (K. Gavril), [schiftner@evolute.at](mailto:schiftner@evolute.at) (A. Schiftner), [pottmann@geometrie.tuwien.ac.at](mailto:pottmann@geometrie.tuwien.ac.at) (H. Pottmann)

system cannot be solved in a simple way, but in various special cases, explicit solutions have been derived ([2, 3, 4, 5]). One can avoid these nonlinear constraints by using the projectively dual representation, where a developable is represented as the envelope of its tangent planes. For details, we refer to [6], but note that the dual representation is not sufficiently intuitive to be suitable for interactive design. Moreover, it is difficult to control singularities. A combination of the primal and the dual representation has been successfully employed for interactive design of developable NURBS surfaces by Tang et al. [7].

*Discrete representations and nearly developable surfaces.* There are numerous papers which model developable surfaces with triangle meshes; we just refer to a few of them [8, 9, 10, 11]. Jung et al. [12] improve on Decaudin et al.’s [13] method that locally approximates neighborhoods around each mesh triangle with a cone. Liu et al. [14] treat developable surfaces as a limit case of meshes from planar quads. Solomon et al. [15] use a mesh approach to flexibly model the shapes achievable by bending and folding a given planar domain without stretching or tearing. An elegant discrete model of developable surfaces is provided by special quad meshes which discretize orthogonal nets of geodesics [16].

Nearly developable surfaces appear in connection with specific applications, e.g. modeling ship hulls [17] and clothing [18] or segmenting meshes in geometry processing [19, 20]. Narain et al. [21] go beyond developability and present a technique for simulating plastic deformation in sheets of thin materials, such as crumpled paper, dented metal, and wrinkled cloth. Closely related to our work is a paper by Wang et al. [22] on increasing developability of a trimmed NURBS surface, but our approach and applications differ significantly.

Another very recent work with a strong connection to our research is the developable surface flow by Stein et al. [23]. This flow is a gradient flow on the energy  $\int_M \kappa_1^2 dA$ ,  $\kappa_1$  being the smallest principal curvature. It admits piecewise rather than globally developable surfaces as minimizers. The discrete model is based on triangulations whose vertex stars dominantly lie in pairs of planes. One could say that the surface is locally approximated by a pair of planes, their intersection representing the ruling direction. In a similar spirit, our local approximations are of higher order, as discussed below.

*Paneling architectural surfaces.* Architectural surfaces need to be decomposed into panels, which is a key process and largely responsible for a cost effective solution. For an overview of the problems in this field we refer to [24]. In particular, we point to the paneling solution of Eigensatz et al. [25]. It exploits various tolerances at seams and a cost model for the production of panels of different geometric types to suggest solutions within an optimization framework. The user provides the design surface and a suggested network of panel boundary curves, while the algorithm slightly adapts the design surface and network and optimally fills it with panels (patches). Our work can be considered as an extension in the sense that the panel boundaries are also subject to optimization with the overall goal of increasing developability of the individual panels. For developable and nearly developable surfaces in architecture, we further point to [26, 27, 28, 29].

**Contributions.** The main contributions of this paper are as follows:

- We present a novel optimization method for increasing the developability of an arbitrary surface. It is based on local approximations of the surface by developable surfaces with planar and thus circular Gauss images. While we could also use other representations within our framework, we prefer B-splines in order to have simple access to smoothness of patches. Moreover, we naturally obtain a patchwork of regular quad combinatorics, which is a preferred arrangement in many architectural projects.
- We provide a justification of our approach in two ways: We discuss local approximations of developable surfaces, especially with those being characterized by a planar Gauss image. Moreover, we study the implications of a nearly curve-like Gauss image on the underlying surface, thus supporting our claim of achieving near developability through Gauss image thinning.
- We introduce a variation of the main method presented in the paper to tackle the problem of paneling a freeform surface with (rotational) cylindrical, (rotational) conical and planar panels, which are the main preferred types of developable panels in architecture due to the reduced cost of manufacturing.

- We provide results that illustrate the power of the proposed approach and outline potential directions for future research.

**Overview of the paper.** This paper is organized as follows. In Section 2, we outline some important fundamentals for our work and, in section 3 present the main optimization algorithm step by step. Section 4 focuses on a variation of the main optimization algorithm which is designed for paneling a freeform surface with panels that are special cases of developable surfaces. We present the differences with the main algorithm and introduce any necessary new tools. In section 5, we provide results on various data sets, including ones from real architectural projects. Moreover, we discuss advantages and shortcomings of our approach and outline future work.

## 2. Fundamentals

### 2.1. Local approximations of developable surfaces

We are interested in smooth or piecewise smooth developable surfaces  $S$ . They are composed of  $C^2$  surface patches which fall into one of the following four categories: planes, general cylinders, general cones and tangent surfaces of space curves. Their *Gauss images*  $C$ , i.e. sets of unit normals viewed as points on the unit sphere  $S^2$ , are composed of *curves*. The junction points of  $C$  where more than two curve segments meet, correspond to planar patches on  $S$ . In the following, we discuss only the three non-trivial basic types: These are ruled surfaces with a constant tangent plane along each ruling. In other words, they are envelopes of a one-parameter family of planes.

We are interested in second order local approximations of these basic types. The following result is well-known (see, e.g. [6]) and closely related to the simple fact that the Gauss image of a developable surface is a spherical curve, which has an osculating circle at each of its regular points.

**Lemma 2.1.** *Along each ruling  $r$ , a non-planar developable ruled surface  $S$  has second order contact with a rotational cone  $\Gamma$  (osculating cone). The vertex of this cone is the singular point of  $r$  (regression point).  $\Gamma$  is a rotational cylinder for a cylindrical ruling  $r$  (regression point at infinity) and it degenerates to a plane if  $r$  is an inflection ruling.*

The Gauss image of a rotational cone  $\Gamma$  is a circle  $C$  on  $S^2$  which becomes a great circle if  $\Gamma$  is a cylinder and degenerates to a point for a plane  $\Gamma$ . So all 2nd order local approximations addressed above have a *planar Gauss image* curve  $C$ . However, a planar Gauss image  $C$  of a surface  $\Gamma$  does not yet imply that  $\Gamma$  is a cone, while  $\Gamma$  must be a cylinder if  $C$  is a great circle and a plane if  $C$  is just a point. So let us discuss the case of a small circle  $C$  as Gauss image of a surface. These surfaces are well studied in classical differential geometry and known as *surfaces of constant slope*. They are the tangent surfaces of curves  $c$  of constant slope. Their tangents form a constant angle with a certain direction in space, which is obviously the rotational axis of the circle  $C$ . For a detailed study of these surfaces, we refer to [6]. Interestingly, we can prove the following result:

**Theorem 2.2.** *At each regular point  $p$  of a developable ruled surface  $S$ , there is a developable surface  $\Gamma$  with a planar Gauss image, which has third order contact with  $S$  at  $p$  and second order contact with  $S$  along the entire ruling through  $p$ .*

*Proof.* We only sketch the main steps of the proof and omit the obvious cases where  $S$  is a plane or a cylinder, since these surfaces already have a planar Gauss image curve. So we are left with cones and tangent surfaces  $S$ . We pick the osculating cone  $\Gamma_p$  of  $S$  along the ruling  $r_p$  through  $p$ . It has a certain conic at infinity  $c_\infty$ . Moreover, we take any curve  $a \subset S$  through  $p$  which is transversal to the rulings. The two curves  $c_\infty$  and  $a$  possess a connecting developable surface  $\Gamma$  which has second order contact with  $S$  along the ruling  $r_p$  (with  $\Gamma_p$  as the common osculating cone along  $r_p$ ). One can then show that  $S$  and  $\Gamma$  possess parametrizations of the following form:

$$\mathbf{S}(u, v) = \mathbf{a}(u) + v\mathbf{r}(u), \quad \Gamma(u, v) = \mathbf{a}(u) + v\bar{\mathbf{r}}(u).$$

Here, the point  $p$  belongs to  $(u, v) = (0, 0)$  and  $\mathbf{a}(u)$  parametrizes the curve  $a$  for both surfaces in the same way, while the ruling vectors  $\mathbf{r}(u)$  and  $\bar{\mathbf{r}}(u)$  only agree up to second order at  $u = 0$ . Thus, the claim on the third order contact at  $p$  requires the 3rd order derivatives of these parameterizations,

$$\mathbf{S}_{uuu} = \ddot{\mathbf{a}} + v\ddot{\mathbf{r}}, \quad \mathbf{S}_{uuv} = \ddot{\mathbf{r}}, \quad \mathbf{S}_{uvv} = \mathbf{S}_{vvv} = 0,$$

and likewise for  $\Gamma$ , which obviously agree at  $(u, v) = (0, 0)$ . We also see that there is in general no third order contact along the entire ruling  $r_p$ . Even if  $S$  is a cone,  $\Gamma$  is in general not a cone.

Knowing that surfaces with a planar Gauss image approximate developable surfaces at each point to third order, we can increase developability by enforcing local approximations of this type through an optimization algorithm (see section 3).

## 2.2. Surfaces with a thin Gauss image

Our method will try to make the Gauss image of a B-spline surface thinner. After that, it will lie in a region  $R_\varepsilon$  on the sphere which has at most geodesic distance  $\varepsilon$  to a curve  $C \subset S^2$ . Let us briefly discuss the implications on a surface  $S$  which has a Gauss image in such an  $\varepsilon$ -strip  $R_\varepsilon$ . For that, we pick a part of the surface without an umbilic; there the principal curvature lines form a quadrilateral curve network without singularities. For simplicity, let us just consider a patch  $\mathcal{P} \subset S$  in this region which is bounded by four principal curvature lines and does not contain parabolic points. Moreover, we select a square-like patch  $\mathcal{P}$ , meaning that the average length of the two pairs of opposite boundary curves is the same. The Gauss image  $\sigma(\mathcal{P})$  of that principal patch  $\mathcal{P}$  is a principal patch on  $S$ ; corresponding curves on  $P$  and  $\sigma(\mathcal{P})$  have parallel tangents at corresponding points, as they are principal directions and thus eigendirections of the derivative of the Gauss map. As we exclude parabolic points in  $\mathcal{P}$ , the Gauss map is regular everywhere and thus locally injective.

The Gauss image  $\sigma(\mathcal{P})$  of  $\mathcal{P}$  is squeezed into the thin region  $R_\varepsilon$ . Being contained in  $R_\varepsilon$ , at least one family  $F_1$  of principal curvature lines on  $\mathcal{P}$  must be mapped to very short curves in  $R_\varepsilon$ . If this is not true for the other family  $F_2$  of principal curvature lines; the Gauss image curves of that family must be nearly parallel to the central curve  $C$  of  $R_\varepsilon$ . Thus, the Gauss images of curves in  $F_1$  will be nearly orthogonal to  $C$  (see Figures 9, 10). Their length can be bounded depending on the width variation of  $\sigma(\mathcal{P})$ . The shortening of curves in  $F_1$  through the Gauss map to a length  $\approx \varepsilon$  implies that the curves themselves will be close to straight lines. A surface with one family of straight principal curvature lines is exactly developable; our surface is only an approximation of that. A more thorough investigation of the geometric implications of a thin Gauss is left for future research.

Due to our focus on architectural geometry, we can exclude surfaces with wrinkles or folds appearing for example in cloth. These wrinkles are close to curves formed by parabolic points and have one very high principal curvature. They are not of interest in the present paper, and are not characterized by thin Gauss images. Some insight into the geometry of these folds can be obtained as follows: Consider a planar sheet of material, mark a fold curve on it and bend it into a 3D shape  $S$ , leading to a developable surface with a curved crease (for the local geometry of such curved folds, see e.g. ([6])). The two developable surfaces on either side of the fold curve  $f$  have curves  $C_1, C_2$  as Gauss images. Now let us add a thin smooth blend to round off the fold curve  $f$ . The Gauss image of that blend surface will connect the two curves  $C_1, C_2$  to a region which needs not be thin at all. With a sufficiently small blending radius the shape  $S$  can be arbitrarily close to an exact developable surface and thus be nearly developable, but the Gauss image will not be thin.

Therefore, our approach of thinning the Gauss image implies the construction of nearly developable surfaces, but the converse is not true. A nearly developable surface needs not have a thin Gauss image, due to the phenomenon of wrinkles.

## 2.3. Developable bicubic surfaces

We will use bicubic B-spline surfaces and thus it is appropriate to justify this choice. When it comes to modeling nearly developable surfaces, our choice is natural due to the approximation power of splines. The condition of one family of nearly straight principal curvature lines is sufficiently soft to be modeled nicely with these splines.

However, especially in our architectural application, we will model panel arrangements also by bicubic B-spline surfaces, with knots of multiplicity three, which are just  $C^0$  patchworks of bicubic polynomial patches. We want these polynomial patches to be close to developable surfaces, in particular to right circular cones or cylinders. Thus, we briefly discuss *developable bicubic surfaces*.

**Bicubic patches on tangent surfaces.** The tangent surface of a polynomial cubic  $\mathbf{c}(u)$  can be parameterized as

$$\mathbf{x}(u, v) = \mathbf{c}(u) + v\dot{\mathbf{c}}(u),$$

and it is therefore a bicubic surface. In this form, the rulings are  $v$ -isoparameter curves and an axis aligned rectangle in the parameter domain represents a patch on the surface bounded by two rulings. There are other bicubic patches on that surface, which are obtained as images of arbitrary parallelograms in the  $(u, v)$ -plane. Equivalently, one can obtain them as images of the unit square  $[0, 1]^2$  in a  $(\bar{u}, \bar{v})$  parameter plane via an affine parameter change,

$$u = a_0 + a_1 \bar{u} + a_2 \bar{v}, \quad v = b_0 + b_1 \bar{u} + b_2 \bar{v}.$$

Furthermore, special bilinear re-parameterizations where the first equation remains and the second one reads

$$v = b_0 + b_1 \bar{u} + b_2 \bar{v} + b_3 \bar{u} \bar{v},$$

also yield bicubic patches on that tangent surface.

Even the tangent surface of a polynomial quartic  $\mathbf{c}(u)$  has a bicubic parameterization. We write  $\mathbf{c} = \mathbf{a}_4 u^4 + \mathbf{a}_3 u^3 + \dots + \mathbf{a}_0$  in monomial form and parameterize its tangent surface as

$$\mathbf{x}(u, v) = \mathbf{c}(u) + (-u/4 + v)\dot{\mathbf{c}}(u),$$

which is a bicubic representation. A complete classification of all bicubic tangent surfaces is an open problem. For our purposes it suffices to see that tangent surfaces of quartic curves are included in this class of surfaces, which leaves sufficient flexibility for modeling.

**Bicubic patches on cones and cylinders.** A cone with vertex  $\mathbf{v}$  can be written as  $\mathbf{x}(u, v) = \mathbf{v} + f(u, v)\mathbf{c}(u)$ . To get a bicubic parameterization, we can use a cubic curve  $\mathbf{c}(u)$  and a cubic polynomial  $f(u, v) = g(v)$  or a quadratic curve (parabola)  $\mathbf{c}(u)$  and a function  $f(u, v)$  of bi-degree  $(1, 3)$ . In the former case, the cone is in general a cubic surface, while in the latter case one parameterizes quadratic cones.

A cylinder  $\mathbf{x}(u, v) = \mathbf{a}(u) + f(u, v)\mathbf{r}$ , with a ruling direction  $\mathbf{r}$ , has a bicubic representation when  $\mathbf{a}(u)$  is at most cubic and  $f$  any bicubic function.

**Developable bicubic patches with a planar Gauss image.** This class of surfaces includes all bicubic cylinders. Among the cones, only rotational cones are possible. We can generate them from the special cone  $x^2 + y^2 = z^2$ , and then apply uniform scaling in  $z$ -direction and a rigid body motion. The special cone is parameterized by a Pythagorean triple of bicubic functions  $x(u, v), y(u, v), z(u, v)$  of the form

$$x(u, v) = 2abw, \quad y(u, v) = (a^2 - b^2)w, \quad z(u, v) = (a^2 + b^2)w,$$

where  $a(u, v), b(u, v), w(u, v)$  are bilinear functions. Bicubic tangent surfaces with a planar Gauss image have a regression curve  $\mathbf{c}(u)$  of constant slope. It follows from our considerations above that the tangent surface of a polynomial curve  $\mathbf{c}(u)$  of constant slope and degree  $\leq 4$  is such a surface. These curves  $\mathbf{c}(u)$  are exactly the *spatial Pythagorean hodograph curves* of degree  $\leq 4$ . For their generation and degrees of freedom, we point to the monograph by R. Farouki [30].

We have already mentioned rotational cones and note that rotational cylinders do not possess an exact bicubic parameterization. This is due to the fact that a rotational cylinder cannot carry a polynomial curve transversal to the rulings as it would project onto a circle. While a circle does not have an exact polynomial parameterization, it is possible to achieve good approximations with cubics (see [31] and the references therein). This is sufficient for our purposes.

**Developable B-spline surfaces.** If two algebraic developable surface patches meet with  $C^1$  continuity at a common curve (different from a ruling), their set of tangent planes agrees there. Due to the algebraic nature, agreement of the set of tangent planes along a curve segment is sufficient for the agreement of the set of tangent planes everywhere and for agreement of the two algebraic surfaces. Therefore, any developable B-spline surface with  $C^1$  continuity represents a single polynomial developable surface, unless the patches are joined along rulings. This latter case is used in [7]. The former case is useful to represent appropriate trimmed patches on polynomial developable surfaces, but not for increasing the flexibility in modeling the surfaces themselves.

A regular bicubic surface  $\mathbf{S}$  parameterized by parameters  $u, v$  is developable when the Gaussian curvature vanishes at every point  $(u, v) \in D$  of the surface. Based on this definition of developable surfaces, we can compute the algebraic complexity of the developability property for  $\mathbf{S}$ . Since the

Gaussian curvature is the ratio of the determinants of the second and first fundamental forms, it is sufficient for the following equation to hold

$$\det(\mathbf{II}) = 0 \Leftrightarrow [\mathbf{S}_{uu}, \mathbf{S}_u, \mathbf{S}_v][\mathbf{S}_{vv}, \mathbf{S}_u, \mathbf{S}_v] - [\mathbf{S}_{uv}, \mathbf{S}_u, \mathbf{S}_v]^2 = 0, \quad \forall (u, v) \in D$$

where  $[\mathbf{a}, \mathbf{b}, \mathbf{c}]$  denotes the triple product of vectors  $\mathbf{a}, \mathbf{b}, \mathbf{c} \in \mathbb{R}^3$ . Expanding and grouping with respect to monomials in parameters  $u, v$  we get a polynomial  $f \in \mathbb{R}[x_{00}, y_{00}, z_{00}, \dots, x_{33}, y_{33}, z_{33}][u, v]$ , where  $(x_{ij}, y_{ij}, z_{ij}) \in \mathbb{R}^3$ , are the coordinates of control point  $\mathbf{P}_{i,j}$  of surface  $\mathbf{S}$ . Following this grouping, we count that polynomial  $f$  has 191 coefficients  $g_k \in \mathbb{R}[x_{00}, y_{00}, z_{00}, \dots, x_{33}, y_{33}, z_{33}]$ , where  $k = 1, \dots, 191$ .

The requirement that polynomial  $f$  vanishes for all values  $(u, v) \in D$  is satisfied if  $f$  is identically the zero polynomial, or equivalently all coefficient polynomials  $g_k$  vanish. This means that, if we need to guarantee these conditions precisely by evaluating  $f$  at different points on the surface, we would require a minimum of 191 points in a general position, namely points that would generate linearly independent combinations of  $g_k$ . In practice, since  $\deg_u(f) = \deg_v(f) = 13$  we would define a  $14 \times 14$  regular grid over  $D$  to acquire 196 evaluation points.

Alternatively, we can examine the algebraic variety  $V(I)$  of the ideal  $I = \langle g_1, \dots, g_{191} \rangle$  generated by the coefficient polynomials  $g_k$ . Again, these are 191 homogeneous polynomials in 48 variables with  $\deg(g_k) = 6$ . Computing a reduced Gröbner basis in an attempt to work with a minimal number of generators  $h_m \in \mathbb{R}[x_{00}, y_{00}, z_{00}, \dots, x_{33}, y_{33}, z_{33}]$ , with  $m \leq 191$ , for the ideal  $I$  is computationally expensive, and is expected to produce generators that have increasingly higher degrees, bounded by  $2 \cdot 24^{190}$  [32].

These observations only demonstrate that if we wish to increase interactivity in the design process with developable surfaces, we need to avoid the computational complexity of exact satisfiability and instead sufficiently approximate the developability property in an efficient way.

### 3. Increasing developability

Motivated by Theorem 2.2, we can try to increase the developability of a surface  $S$  as follows: We ensure that the Gauss images of well chosen regions on  $S$  are nearly planar. These local shaping surfaces, characterized by a planar Gauss image, are a generalization of the condition used by Stein et al. [23] in their discrete developable flow: They require that vertex stars in a triangle mesh lie in a pair of planes, which implies that the Gauss image of the star lies on a great circle. Here, we have a smoother version. We do not work with triangle meshes, but with smooth surfaces, and we optimize just for planarity of the Gauss images of appropriate regions on the surface.

We now discuss the details of an optimization algorithm which iteratively deforms a bicubic B-spline surface towards a nearly developable one.

#### 3.1. Optimization setup

**Surface.** Let us consider a bicubic B-spline surface  $\mathbf{S} : \mathbb{R}^2 \rightarrow \mathbb{R}^3$ ,

$$\mathbf{S}(u, v) = \sum_{i=0}^n \sum_{j=0}^m B_{i,3}(u) B_{j,3}(v) \mathbf{P}_{i,j}, \quad (1)$$

where  $u, v \in [0, 1]$  and  $B_{i,3}(u), B_{j,3}(v)$  are cubic B-spline basis functions defined on uniform knot sequences in both directions.  $\{\mathbf{P}_{i,j}\} \in \mathbb{R}^3$  are the control points of the surface  $\mathbf{S}$ , where  $0 \leq i \leq n$ ,  $0 \leq j \leq m$  and  $n, m \geq 3$ . For more information on B-spline surfaces and NURBS surfaces in general, we direct the reader to [33].

Surface  $\mathbf{S}$  serves as the central object of study in this work. A generic surface of the above form is non-developable and we aim to increase its developability by modifying the coordinates of its control points in a "minimal" way that will be defined in the following sections.

We point out that surface  $\mathbf{S}$  could be defined as any NURBS surface as long as the weights of the control points and the knot vectors are fixed and are not considered variables in the optimization process. This simplifies and accelerates the optimization procedure while not sacrificing the quality of our results in the sense that B-spline surfaces are adequate approximations of more general NURBS surfaces. For readability, we define  $\mathbf{S}$  as an elementary B-spline surface while keeping in mind that the following applies to more general surfaces.

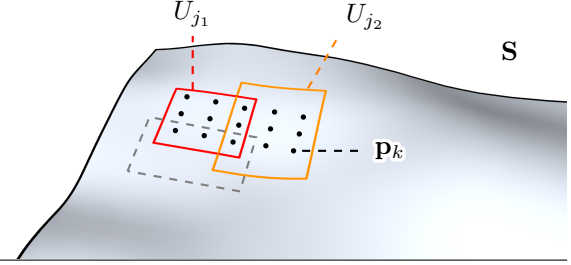
**Sampling the surface.** We begin by sampling  $\mathbf{S}$ , the surface that is to be optimized, at a set of evaluation points  $\{\mathbf{p}_k\} \subset \mathbb{R}^3$ , which we will call *sample points*.

The approach we took for the sampling was to uniformly sample the parameter space, motivated by the fact that convoluted areas on the surface  $\mathbf{S}$ , i.e. areas where the control points are concentrated and finer features emerge, would be represented by more evaluation points inherently. We set the number of sample points  $L_u, L_v$  along the  $u, v$  directions respectively and get a gridded pattern of points  $(u, v) \in [0, \frac{1}{L_u+1}, \dots, 1] \times [0, \frac{1}{L_v+1}, \dots, 1]$  on the parameter space, which in turn results in the set of required sample points  $\{\mathbf{p}_k\}$  on the surface  $\mathbf{S}$ .

The evaluation of points  $\mathbf{p}_k$  is given by formula 1, which is linear in the coordinates of the control points with constant coefficients. In practice, these coefficients are precomputed per point and stored. Whenever the control points are updated by the optimization process or user input, we re-evaluate the position of the sample points using the stored coefficients.

**Grouping into patches.** Next, we consider overlapping neighborhoods on the surface, that we will call *patches*, and that are represented as sets of sample points  $U_j$ . We construct the patches in such a way that neighboring patches will have non-empty intersections, i.e. there exists at least one sample point that belongs to both patches. The importance of this property will become clear in a later section.

**Figure 1:** Surface  $\mathbf{S}$  is sampled at various evaluation points  $\mathbf{p}_k$ . The sample points are then grouped to overlapping groups. An example of such a grouping are groups  $U_{j_1}$  and  $U_{j_2}$ .



By uniformly sampling the parameter space we also simplify the process of grouping the sample points. The patches on the surface, as already mentioned, are represented by sets of sample points. By using the grid of points on the parameter space we can determine the patches just by setting the number of sample points in each of the  $u, v$  directions that a patch will contain and the number of sample points that will belong in the overlap region for each of the  $u, v$  directions. Figure 1 focuses on two such patches as an example of a simple grouping.

**Normal computation.** We associate each sample point  $\mathbf{p}_k$  with the unit normal  $\mathbf{n}_k$  of the surface at that point. The unit normals define the *Gauss map*  $\sigma$  of the surface. We compute the unit normal  $\mathbf{n}_k$  of the surface point  $\mathbf{p}_k$  as

$$\mathbf{n}_k := \sigma(\mathbf{p}_k) = \frac{\mathbf{S}_u \times \mathbf{S}_v}{\|\mathbf{S}_u \times \mathbf{S}_v\|},$$

where  $\mathbf{S}_u, \mathbf{S}_v$  are the partial derivatives of  $\mathbf{S}$  with respect to  $u$  and  $v$ . Note that  $\mathbf{S}_u$  and  $\mathbf{S}_v$ ,

$$\mathbf{S}_u(u, v) = \sum_{i=0}^n \sum_{j=0}^m B_{i,3}^{(1)}(u) B_{j,3}(v) \mathbf{P}_{i,j}, \quad \mathbf{S}_v(u, v) = \sum_{i=0}^n \sum_{j=0}^m B_{i,3}(u) B_{j,3}^{(1)}(v) \mathbf{P}_{i,j},$$

are linear combinations of the control points with coefficients which we precompute and store to accelerate future computations [33].

**Gauss map of a patch.** For every patch  $U_j$ , we denote by  $N_j$  the Gauss image of  $U_j$ , i.e. the set of unit normals  $\mathbf{n}_k$  corresponding to the sample points  $\mathbf{p}_k \in U_j$ ,

$$N_j = \sigma(U_j) = \sigma(\{\mathbf{p}_k\}) = \{\mathbf{n}_k\}.$$

We associate each patch  $U_j$  with a plane  $H_j \subset \mathbb{R}^3$  with equation  $\mathbf{v}_j \cdot \mathbf{x} + d_j = 0$ . Here,  $\mathbf{v}_j$  is a unit normal vector of  $H_j$  and  $d_j$  is the distance of  $H_j$  from the origin.  $H_j$  serves as the target plane

for  $N_j$ . By optimization, we will enforce all normal vectors in  $N_j$  to lie on  $H_j$  and thus aim at a planar Gauss image of patch  $U_j$ .

### 3.2. Initialization

The variables of the optimization are the coordinates of the control points  $\mathbf{P}_{i,j}$  and the cutting planes  $H_j$  that define the Gauss image circles per patch  $U_j$ . In this section, we describe the initialization step of the optimization process.

**Control points.** We assume that we always have an initial state for the surface that is either user defined or is provided by other means. We initialize the control point coordinates with the values from this initial configuration. Those in turn will be used to initialize  $H_j$  for every patch.

**Cutting planes.** We want to optimize for planarity of the Gauss image  $N_j$  of each patch  $U_j$  and thus associate with each patch  $U_j$  a target plane  $H_j$  for  $N_j$ . Initializing the target plane  $H_j$  for each patch with the best fitting plane to points  $\mathbf{n}_k \in S^2$  works in the case that  $U_j$  is a developable patch. However, this method does not produce the desired results if the patch is non-developable, as seen in Figure 2. To overcome this, we use the following approach.

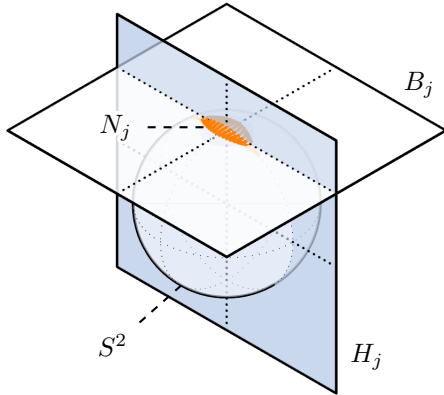


**Figure 2:** Plane  $B_j$  is the best fitting plane to the set of points in  $N_j$ , in the sense that it minimizes the sum of squared distances of the points to the plane, and is considered an undesired initialization. Alternatively, plane  $H_j$  is the resulting plane from optimization problem 1 and captures the overall main principal direction of patch  $U_j$ .

Consider the main principal direction  $\mathbf{q}_k \in \mathbb{R}^3$  of surface  $\mathbf{S}$  at point  $\mathbf{p}_k$ , i.e. the principal direction corresponding to the principal curvature with the maximum absolute value, that is  $\max\{|\kappa_1(\mathbf{p}_k)|, |\kappa_2(\mathbf{p}_k)|\}$  where  $\kappa_i : \mathbf{S} \rightarrow \mathbb{R}$ ,  $i = 1, 2$ , are the principal curvatures of a point on  $\mathbf{S}$ . The *principal curvatures* and *principal directions* of a surface at a point on the surface are the eigenvalues and corresponding eigenvectors of the *shape operator*  $-d_v \mathbf{N} = -\mathbf{I}^{-1} \mathbf{II}$ , where  $\mathbf{I}$ ,  $\mathbf{II}$  are the *first* and *second fundamental forms* of the surface. We denote by  $Q_j$  the set of main principal directions  $\mathbf{q}_k$  corresponding to the points  $\mathbf{p}_k \in U_j$ .

We initialize  $H_j$  as the plane passing through the barycenter of  $N_j$  with unit normal in the direction of the vector which is "as orthogonal as possible" to the set  $Q_j$  of main principal directions. Intuitively, we wish the initial cutting plane to intersect the sphere at a circle whose tangent at every point  $\mathbf{c} \in S^2 \cap H_j$  is "as parallel as possible" to the main principal directions of the sample points corresponding to the unit normals around  $\mathbf{c}$ .

In this way, the cutting plane serves as a generalized main principal plane, or a plane containing the main principal directions of every sample point in the patch. For a patch that is non-developable, we wish to initialize this main principal plane by using the main principal directions of the sample points weighted by a measure of confidence. A low weight indicates the difficulty in distinguishing between the two principal curvatures. Specifically, we introduce weight  $w_k \in [0, 1]$  corresponding to each sample point  $\mathbf{p}_k$  as

$$w_k = 1 - \frac{\min\{|\kappa_i(\mathbf{p}_k)|\}}{\max\{|\kappa_i(\mathbf{p}_k)|\}}, \quad i = 1, 2 \quad (2)$$

Now, for each patch  $U_j$  we need to solve the following optimization problem.

---

### Optimization problem 1 Plane initialization

---

$$\begin{aligned} \text{minimize} \quad & \sum_{\mathbf{q}_k \in Q_j} w_k (\mathbf{v}_j \cdot \mathbf{q}_k)^2 \\ \text{subject to} \quad & \mathbf{v}_j^2 = 1 \end{aligned}$$


---

Optimization problem 1 is a special case of minimizing a quadratic form under a quadratic regularization constraint. Bringing the objective function into the form  $\mathbf{v}_j^\top \mathbf{Q} \mathbf{v}_j$ , the minimizer  $\mathbf{v}_j^*$  is the normalized eigenvector corresponding to the smallest eigenvalue of  $\mathbf{Q}$ . Then, plane  $H_j$  is given by  $\mathbf{v}_j^* \cdot \mathbf{x} + d_j = 0$ , with

$$d_j = -\mathbf{v}_j^* \cdot \frac{1}{|N_j|} \sum_{\mathbf{n}_k \in N_j} \mathbf{n}_k,$$

where  $|N_j|$  is the cardinality of  $N_j$ .

### 3.3. Problem formulation

---

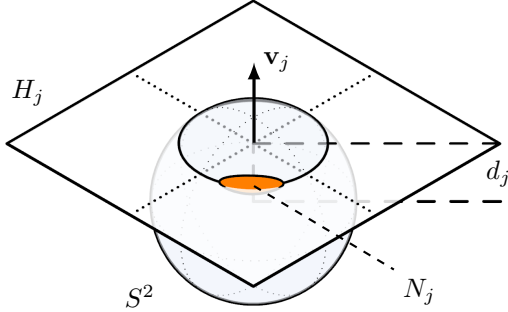


**Figure 3:** The Gauss image  $N_j$  of a single non-developable patch  $U_j$  is a 2-dimensional subset of  $S^2$ . The cutting plane  $H_j$  serves as the target plane for the normals  $\mathbf{n}_k \in N_j$ .

**Developability energy.** We are now ready to formulate the desired property of each patch to have a planar Gauss image by introducing an appropriate energy term  $E_d$ . This energy term measures per patch the total sum of distances of the normals  $\mathbf{n}_k \in S^2$  to the target patch plane, that is the quantity

$$\sum_j \sum_{\mathbf{n}_k \in N_j} (\mathbf{n}_k \cdot \mathbf{v}_j + d_j)^2, \quad (3)$$

where  $j$  is the indexing of the patches and  $\mathbf{v}_j, d_j$  are unit normal and distance from the origin of target plane  $H_j$  for patch  $U_j$ . To avoid trivial solutions, we introduce the following unit length constraint on the plane normals  $\mathbf{v}_j$  in the form of an additional energy term,

$$\sum_j (\mathbf{v}_j^2 - 1)^2.$$

Additionally, the surface normals  $\mathbf{n}_k$  are computed as

$$\mathbf{n}_k^{(m)} = \frac{\mathbf{S}_u^{(m)} \times \mathbf{S}_v^{(m)}}{\|\mathbf{S}_u^{(m-1)} \times \mathbf{S}_v^{(m-1)}\|},$$

where  $a^{(m)}$  denotes the value of variable  $a$  at iteration step  $m$  in our iterative optimization process. We use the constant norm  $\|\mathbf{S}_u^{(m-1)} \times \mathbf{S}_v^{(m-1)}\|$  from the previous iteration when normalizing the current vector  $\mathbf{S}_u^{(m)} \times \mathbf{S}_v^{(m)}$  for the computation of the surface normal  $\mathbf{n}_k$ . This is standard practice to ensure that the objective function is polynomial.

All the above lead to an energy term of the form

$$E_d = \sum_j \sum_{\mathbf{n}_k \in N_j} (\mathbf{n}_k \cdot \mathbf{v}_j + d_j)^2 + \lambda_1 \sum_j (\mathbf{v}_j^2 - 1)^2, \quad (4)$$

where  $\lambda_1$  is an appropriate weight for the unit length constraint.

The importance of having patches that are overlapping, or equivalently neighboring patches containing common sample points, becomes evident at this point. Each patch is optimized to have a Gauss image which is a subset of a spherical curve. This can have a competitive effect between patches that are adjacent due to diverging target planes, and cause slow convergence. By having the patches share sample points, we introduce a diffusion factor to the optimization that ensures smoothness of the resulting Gauss image curve.

**Soft constraints.** We also introduce a set of additional energy terms to the main problem that constrain the output surface and aim to avoid degeneracies, produce more aesthetically pleasing results and give control to the user over the proximity of the resulting surface to a reference surface.

The energy term  $E_c$  denotes a measure of the closeness of the resulting surface  $\mathbf{S}$  to a reference surface  $\mathbf{S}_{\text{ref}}$ , which can be either an arbitrary surface or the initial configuration of the design surface. The implementation we follow for the closeness energy term is based on the *tangential distance minimization* (TDM) [34, 35]. The energy term is defined as the sum of squared distances of sample points to the tangent planes at their closest points on the reference surface. We use the already sampled points  $\mathbf{p}_k \in \mathbf{S}$  and a set of sample points  $X$  from the reference surface  $\mathbf{S}_{\text{ref}}$ . If the reference surface is the initial surface then  $X = \{\mathbf{p}_k\}$ ; otherwise,  $X$  is an independent sampling. Then  $E_c$  is defined as

$$E_c = \sum_k [(\mathbf{p}_k - \mathbf{x}_k) \cdot \mathbf{N}(\mathbf{x}_k)]^2, \quad (5)$$

where  $\mathbf{x}_k$  is the closest point to  $\mathbf{p}_k$  from the set of points  $X$  in the Euclidean metric, and  $\mathbf{N}(\mathbf{x}_k)$  is the unit normal of  $\mathbf{S}_{\text{ref}}$  at point  $\mathbf{x}_k$ . At each iteration the closest point is updated.

A final fairness energy term  $E_f = w_{f_1} E_{f_1} + w_{f_2} E_{f_2}$  is introduced to the objective function that avoids degeneracies in the resulting surface and is widely used in mesh optimization problems for the smoothing effect it provides. Specifically, we denote by  $E_{f_1}$  the sum of squared norms of the first order differences of the control points in both grid directions, and by  $E_{f_2}$  the second order equivalent, namely

$$\begin{aligned} E_{f_1} &= \sum_{i,j} (\|\mathbf{P}_{i+1,j} - \mathbf{P}_{i,j}\|^2 + \|\mathbf{P}_{i,j+1} - \mathbf{P}_{i,j}\|^2), \\ E_{f_2} &= \sum_{i,j} (\|\mathbf{P}_{i+1,j} - 2\mathbf{P}_{i,j} + \mathbf{P}_{i-1,j}\|^2 + \|\mathbf{P}_{i,j+1} - 2\mathbf{P}_{i,j} + \mathbf{P}_{i,j-1}\|^2). \end{aligned}$$

We assign  $w_{f_1} = 0$ ,  $w_{f_2} = 1$  in all the following applications unless stated otherwise.

**Total energy.** All energy terms  $E_d$ ,  $E_c$ ,  $E_f$  are assigned weights  $w_d$ ,  $w_c$ ,  $w_f$  and collected in the total energy for developability optimization,

$$E = w_d E_d + w_c E_c + w_f E_f. \quad (6)$$

For details on the choice of weights, we refer to Section 5.

**Increasing developability.** Now our problem is reduced to the minimization of  $E$ .

---

## Optimization problem 2 Increasing developability

---

$$\text{minimize } E = w_d E_d + w_c E_c + w_f E_f$$


---

The variables of  $E$  are the control points  $\{\mathbf{P}_{i,j}\}$  of  $\mathbf{S}$  and the patch planes  $H_j$ , defined by  $\mathbf{v}_j$  and  $d_j$ . The optimization problem 2 is an unconstrained nonlinear least-squares problem. Any algorithm for nonlinear least-squares problem can be applied in our case. We follow the standard *Gauss-Newton method* in our implementation and experiments [36].

## 4. Panelization

Motivated by applications in architecture, we consider the problem of approximating a given arbitrary surface by a  $C^0$  continuous surface which consists of developable patches. As we optimize for developability with help of a planar Gauss image, the resulting surface patches include as important special cases rotational cylinders and rotational cones. We will particularly focus on the constraints which ensure that we obtain these special types of panels. Especially when working with glass, these rotational panels are preferred because there are special machines for their production. Figure 4 shows a recent example of an architectural freeform facade which has been constructed with mainly cylindrical glass panels to reduce manufacturing cost.



**Figure 4:** Side detail of *Nur Alem*, the main pavilion of the Astana EXPO 2017 Exhibition in Astana, Kazakhstan. Mostly cylindrical panels were used to rationalize the curved transparent freeform façade (different from the sphere).

In this section, we will go through the differences between the central method that was presented in the previous sections and the variation for this new problem while introducing any new concepts that will be of use.

**Surface.** The main object of study in this section will be a surface  $\mathbf{S}$  consisting of a grid of subsurfaces  $\mathbf{S}^{(r)}$ , with  $C^0$  continuity at the inner boundaries. Specifically,  $\mathbf{S}$  is a composite surface

$$\mathbf{S} = \bigcup_r \mathbf{S}^{(r)},$$

where  $r$  indexes the set of subsurfaces. Each  $\mathbf{S}^{(r)}$  is a bicubic Bézier surface of the form

$$\mathbf{S}^{(r)}(u, v) = \sum_{i=0}^3 \sum_{j=0}^3 B_{i,3}(u) B_{j,3}(v) \mathbf{P}_{i,j}^{(r)} \quad (7)$$

and will be referred to as a *panel* in the following. This configuration represents the paneling of a freeform surface. The  $C^0$  continuity of neighboring panels is achieved by having common control points at the corresponding edges and models the connectivity and continuity found between distinct panels of a panelized surface.

An equivalent formulation of surface  $\mathbf{S}$  would be to consider a bicubic B-spline surface as in (1), but with knot multiplicity 3 to achieve the desired  $C^0$  continuity of the bicubic segments. We will not follow this formulation but rather treat each panel as a distinct element. This allows for panelizations that are not in a grid configuration and can easily generalize to more complex surfaces of arbitrary topology just by appropriately "gluing" panels at their edges.

**Sampling and grouping.** We sample surface  $\mathbf{S}$  at a collection of sample points  $\{\mathbf{p}_k\}$  in a similar manner to the main algorithm of the paper, described in section 3. The key difference with the main optimization problem is that the grouping of the sample points  $\{\mathbf{p}_k\}$  is with respect to the panel they belong to, meaning we view every panel as a single patch from the setup described in section 3.1. Notice that this restriction does not allow for any overlap of the sample point sets. Instead, the grouping  $\{U_r\}$  constitutes a partition of the sample points, such that each set  $U_r$  corresponds to a single panel. The same is true for the grouping of the corresponding surface normals  $N_r$  and the associated panel planes  $H_r$ .

We can therefore define the developability energy term per panel as

$$E_d^{(r)} = \sum_{\mathbf{n}_k \in N_r} (\mathbf{n}_k \cdot \mathbf{v}_r + d_r)^2 + \lambda_1 (\mathbf{v}_r^2 - 1)^2, \quad (8)$$

where  $\lambda_1$  is an appropriate weight, and the developability energy term of surface  $\mathbf{S}$  as

$$E_d = \sum_r E_d^{(r)}. \quad (9)$$

The panel normals  $\mathbf{n}_k$  are again computed using the previous iteration norm of the cross product as in 4.

This modified grouping of the sample points  $\{\mathbf{p}_k\}$  allows for the individual optimization of each panel, which will be studied in more detail in a following section. By optimizing for the sample unit normals of each of the  $U_r$  to lie on the corresponding  $H_r$ , we are optimizing for the Gauss image of each panel to be a subset of a circle of  $S^2$ .

**Rotational panels.** By introducing the additional constraint that the panel should be a rotational surface, we are optimizing for the panels to be either rotational cones or rotational cylinders. Rotational surfaces have the property that the surface normal lines are coplanar with the axis of rotation. Let  $L_1, L_2$  be two lines in  $\mathbb{R}^3$  with Plücker coordinates  $(\mathbf{a}, \bar{\mathbf{a}}), (\mathbf{b}, \bar{\mathbf{b}}) \in \mathbb{R}^6$  respectively. The two lines are coplanar if their Plücker coordinates satisfy the condition

$$\mathbf{a} \cdot \bar{\mathbf{b}} + \bar{\mathbf{a}} \cdot \mathbf{b} = 0. \quad (10)$$

Recall that the Plücker coordinates  $(\mathbf{a}, \bar{\mathbf{a}}) \in \mathbb{R}^6$  of a line  $L \subset \mathbb{R}^3$  are given by the direction vector  $\mathbf{a} \in \mathbb{R}^3$  and the moment vector  $\bar{\mathbf{a}} = \mathbf{p} \times \mathbf{a} \in \mathbb{R}^3$ , where  $\mathbf{p} \in \mathbb{R}^3$  is a point on  $L$ . Obviously, these coordinates are not independent, but satisfy the Plücker condition  $\mathbf{a} \cdot \bar{\mathbf{a}} = 0$ . For more information on line geometry and relevant applications, we refer to the literature [6].

Consider now the Plücker coordinates  $(\mathbf{n}_k, \bar{\mathbf{n}}_k) \in \mathbb{R}^6$  of the normal lines at the sample points of a panel  $U_r$  and of the unknown axis of rotation  $(\mathbf{a}_r, \bar{\mathbf{a}}_r) \in \mathbb{R}^6$ . The desired property that the panel is a rotational surface can be expressed as  $\mathbf{a}_r \cdot \bar{\mathbf{n}}_k + \mathbf{n}_k \cdot \bar{\mathbf{a}}_r = 0 \forall \mathbf{n}_k \in N_r$ . Thus, the problem of optimizing for rotational surface panels can be formulated as minimizing the energy

$$\sum_r \sum_{\mathbf{n}_k \in N_r} (\mathbf{a}_r \cdot \bar{\mathbf{n}}_k + \mathbf{n}_k \cdot \bar{\mathbf{a}}_r)^2, \quad (11)$$

under the constraint that  $(\mathbf{a}_r, \bar{\mathbf{a}}_r)$  describe a line, i.e., satisfy the Plücker condition  $\mathbf{a}_r \cdot \bar{\mathbf{a}}_r = 0$ , and the unit length constraint  $\mathbf{a}_r^2 = 1$  on the axis direction  $\mathbf{a}_r$ .

At this point, we focus on the fact that for a rotational panel  $S^{(r)}$  with planar Gauss image, the normal  $\mathbf{v}_r$  of the plane  $H_r$  containing the Gauss image and the direction of the rotation axis  $\mathbf{a}_r$  coincide. Using this fact, we denote the Plücker coordinates of the rotation axis by  $(\mathbf{v}_r, \bar{\mathbf{v}}_r)$ .

By making this adaptation, we have covered the unit length constraint on the rotation axis direction by the corresponding constraint on the target plane normal in (8). The Plücker condition is added as an additional energy term with an appropriate weight  $\lambda_2$ . Considering all the above, the resulting rotationality energy term  $E_r$  is of the form

$$E_r = \sum_r \sum_{\mathbf{n}_k \in N_r} (\mathbf{v}_r \cdot \bar{\mathbf{n}}_k + \mathbf{n}_k \cdot \bar{\mathbf{v}}_r)^2 + \lambda_2 \sum_r (\mathbf{v}_r \cdot \bar{\mathbf{v}}_r)^2. \quad (12)$$

While the Plücker coordinates of the normal lines are initialized in the optimization problem with their current values in the configuration of surface  $\mathbf{S}$ , the axis of rotation  $(\mathbf{v}_r, \bar{\mathbf{v}}_r)$  of every panel  $U_r$  remains unknown at this point or, assuming the panels are in generic configuration, does not exist at all. An appropriate initialization for the Plücker coordinates of the axis of rotation of each panel is given by methods used in kinematic surface reconstruction applications, where the problem of fitting a velocity field to a set of surface normals is studied [6, 37, 38]. It follows the same thought process as the main idea behind the energy term (11). In fact, it is exactly the same energy that we aim to minimize but applied to each of the panels separately while considering the affine normal lines fixed. The resulting axis is the best fitting one in the least-squares sense. Formulating the above as an optimization problem leads us to the minimization of

$$\sum_{\mathbf{n}_k \in N_r} (\mathbf{v}_r \cdot \bar{\mathbf{n}}_k + \bar{\mathbf{v}}_r \cdot \mathbf{n}_k)^2. \quad (13)$$

We already have an appropriate initialization for the target plane normal  $\mathbf{v}_r$ , described in optimization problem 1. Thus, the objective function (13) is a quadratic function of the moment vector  $\bar{\mathbf{v}}_r$ . The latter is orthogonal to  $\mathbf{v}_r$  and therefore can be expressed as

$$\bar{\mathbf{v}}_r = \mu_1 \mathbf{b}_1 + \mu_2 \mathbf{b}_2,$$

where  $\mathbf{b}_1, \mathbf{b}_2 \in \mathbb{R}^3$  form a basis of the plane perpendicular to  $\mathbf{v}_r$ . Substitution into (13) yields a quadratic function in  $\mu_1, \mu_2$  and the optimal values of  $\mu_1, \mu_2$  are the solutions of a linear system.

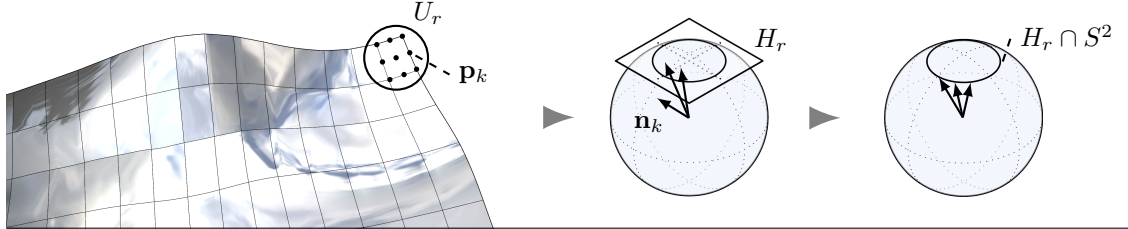


**Figure 5:** We focus on a single panel  $\mathbf{S}^{(r)}$  of a panelized surface  $\mathbf{S}$ . We are optimizing for the endpoints of normals  $\mathbf{n}_k$  corresponding to the sample points  $\mathbf{p}_k \in U_r$  of panel  $\mathbf{S}^{(r)}$  to lie on the same plane  $H_r$ .

**Surface paneling.** Having introduced the adapted grouping methodology for the case of panels and the additional rotational energy term, we can now formulate the surface paneling problem as a variation of optimization problem 2. Specifically, given a grouping  $\{U_r\}$  of the sample points  $\{\mathbf{p}_k\}$  that is per panel, the associated planes  $\{H_r\}$ , and the rotation axes  $(\mathbf{v}_r, \bar{\mathbf{v}}_r)$  we solve the following

---

### Optimization problem 3 Surface paneling

---

$$\text{minimize } E = w_d E_d + w_r E_r + w_c E_c + w_f E_f$$


---

Again, optimization problem 3 is an unconstrained nonlinear least-squares problem and we follow the standard Gauss-Newton method in our implementation to obtain a solution [36].

**Individual panel treatment.** Until now we have shown how to optimize the paneling of surface  $\mathbf{S}$  in a global fashion. Since we defined the energy term  $E_d^{(r)}$  per panel, this approach can be customized to consider each panel separately, achieving in the process increased control over the resulting panelization. We use the following obvious fact:

**Lemma 4.1.** *Let panel  $\mathbf{S}^{(r)}$  be a rotational surface and  $H_r$  be a plane such that the Gauss image of the panel is entirely contained in plane  $H_r$ . Then the panel type is determined by the distance  $d_r$  of plane  $H_r$  from the origin  $O$ . Specifically,*

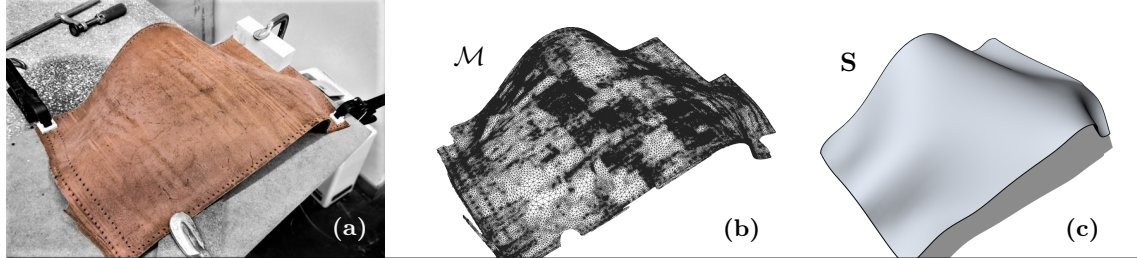
1. *If  $d_r = 1$  then  $\mathbf{S}^{(r)}$  is planar.*
2. *If  $d_r = 0$  then  $\mathbf{S}^{(r)}$  is a cylinder of revolution.*
3. *If  $d_r \in (0, 1)$  then  $\mathbf{S}^{(r)}$  is a cone of revolution whose rulings form the angle  $\arcsin d_r$  with the rotation axis.*

This offers a good way to aim at cylindrical panels or conical panels with prescribed opening angle by prescribing the according values of  $d_r$  in the energy term  $E_d^{(r)}$  in (8).

It is often the case in industrial applications that individual adjustments need to be made to the panelization for reasons that include aesthetics and the overall cost of the project. The advantages of the individual treatment of the panels become apparent in such cases, and the aforementioned main pavilion of the Astana EXPO 2017, shown in Figure 4, serves as an example. In that project, apart from the cylindrical panels which were the main ingredient of the panelization, double curved panels were also utilized in areas that the use of cylindrical panels would negatively affect the aesthetics of the result. Thus, by integrating a singular panel management strategy to the optimization we have the ability of dealing with isolated problematic areas without sacrificing the quality of the overall panelization.

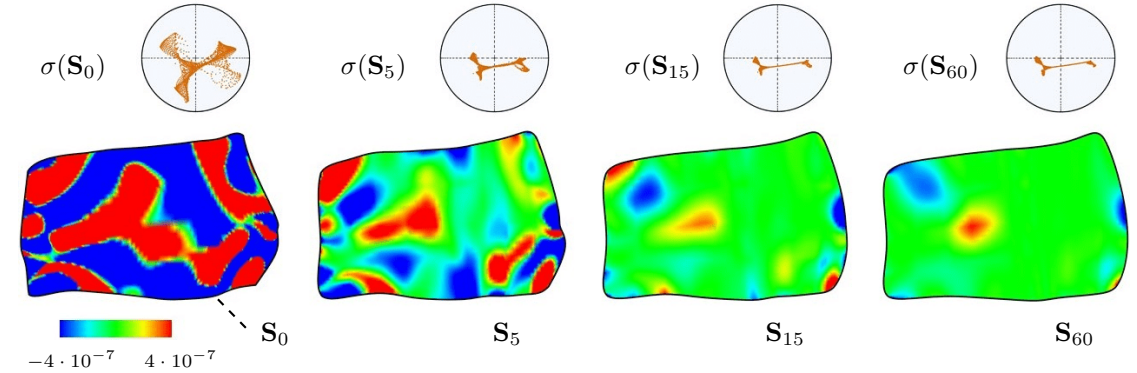
## 5. Experiments, results and discussion

**Example 5.1.** In this example, we consider a mesh  $\mathcal{M}$  which originated from scanning a thin deformed leather patch. The deformation was introduced to the material in the form of local stretches along its surface which result in areas of nonzero Gaussian curvature.



**Figure 6:** (a) The configuration of the deformed leather patch. (b) Mesh acquired from scanning the leather material. (c) The material's geometry is represented as a B-spline surface.

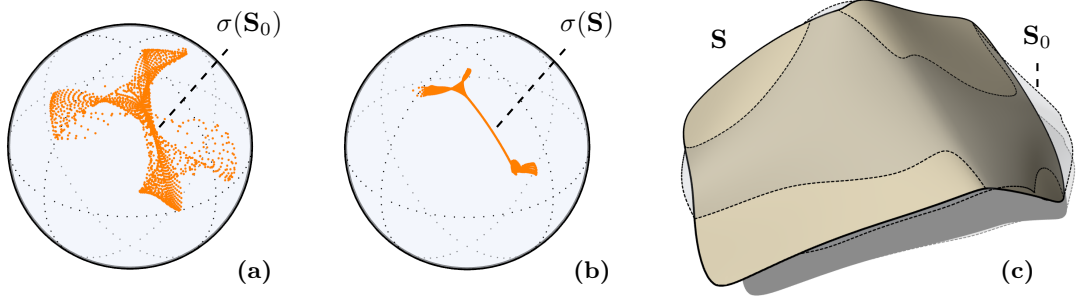
To apply our algorithm for increasing developability, we first fit the data with a bicubic B-spline surface  $\mathbf{S}$  of the form (1) with  $7 \times 13$  control points. This is done using the TDM optimization framework for surface fitting described in section 3.3. We refer to the initial configuration of surface  $\mathbf{S}$ , given by the fitting optimization, as  $\mathbf{S}_0$ . Following the procedure described in section 3.1, we sample the resulting surface  $\mathbf{S}$  uniformly along the parameter space at  $30 \times 60$  evaluation points  $\mathbf{p}_{i,j}$ ,  $i \in [1, 30]$ ,  $j \in [1, 60]$ . We then group  $\mathbf{p}_{i,j}$  in patches  $U_{l,m}$ , each one containing  $5 \times 5$  points with an overlap in both directions of 2 points between neighboring patches, i.e.  $U_{l,m} = \{\mathbf{p}_{i,j} \mid i \in [3l-2, 3l+2], j \in [3m-2, 3m+2]\}$ . This completes the initialization of the optimization algorithm of problem 2.



**Figure 7:** The Gauss map (top) and the Gaussian curvature (bottom) of surface  $\mathbf{S}$  for different numbers of iterations, namely at 0, 5, 15 and 60 ( $\mathbf{S}_t$  denotes the optimized surface at  $t$  iterations). The length of the surface has been scaled to be approximately 1.

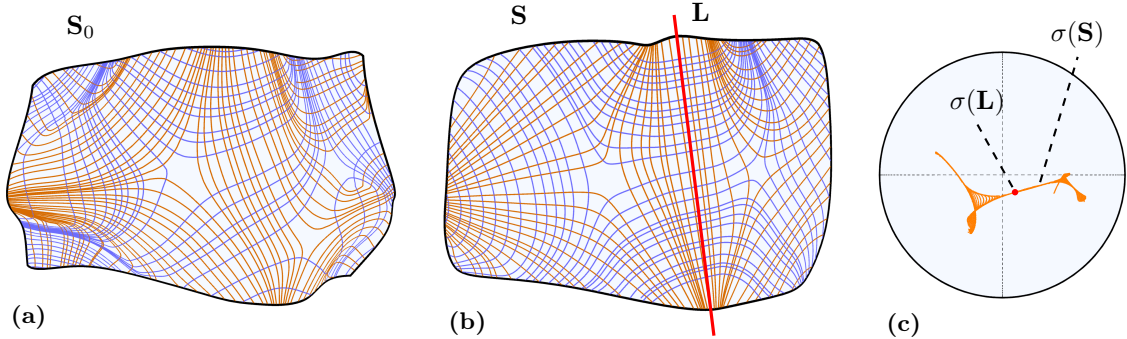
We introduce to the optimization process a closeness energy term of the form (5) with relatively small weight to ensure proximity of  $\mathbf{S}$  to its original position  $\mathbf{S}_0$ . As described before, this is implemented using the TDM framework. We consider the original surface  $\mathbf{S}_0$  as the reference surface and use the already sampled points  $\mathbf{p}_{i,j}$  of surface  $\mathbf{S}$  as the evaluation points of the TDM algorithm. In our experiments, we observed that using this competing low-weight term in our main optimization procedure constrains the solution space by avoiding trivial solutions and producing results that are more desirable from the designer's point of view.

Figure 8 reveals the inner workings of the developability algorithm, which clearly produces a "thinner" Gauss image for the resulting surface and also illustrates a comparison between the original surface  $\mathbf{S}_0$  and the resulting surface  $\mathbf{S}$ . Figure 7 shows the Gauss map and the Gaussian curvature of the surface for several intermediate iterations of the optimization. The detailed statistics for this example are given in Table 1.



**Figure 8:** (a) The Gauss image of the initial configuration of B-spline surface  $S_0$  representing the leather material. (b) The Gauss image of the optimized surface  $S$ . (c) The optimized B-spline surface  $S$  in solid color compared to the transparent initial surface  $S_0$ .

We already discussed in section 2.2 that the straightening of one family of principal curvature lines of surface  $S$  compared to the principal curvature lines of the initial surface  $S_0$  is an alternative indication of the increase in developability. Figure 9 demonstrates the straightening effect in this example. Also illustrated in the same figure is that the preimage of a small collection of points in one of the "thinner" parts of the Gauss image corresponds to one of the approximate rulings of the surface.



**Figure 9:** Visualization of the principal curvature lines. (a) The principal curvature lines of the initial surface  $S_0$ . (b) The principal curvature lines of the optimized surface  $S$ . Highlighted in red and extended slightly for clarity, one such principal curvature line  $L$ , which also approximately corresponds to the preimage of a small collection of points around the "thin" part of  $\sigma(S)$ . (c) The Gauss image  $\sigma(S)$  of the optimized surface  $S$ . The Gauss image of  $L$  is highlighted in red.

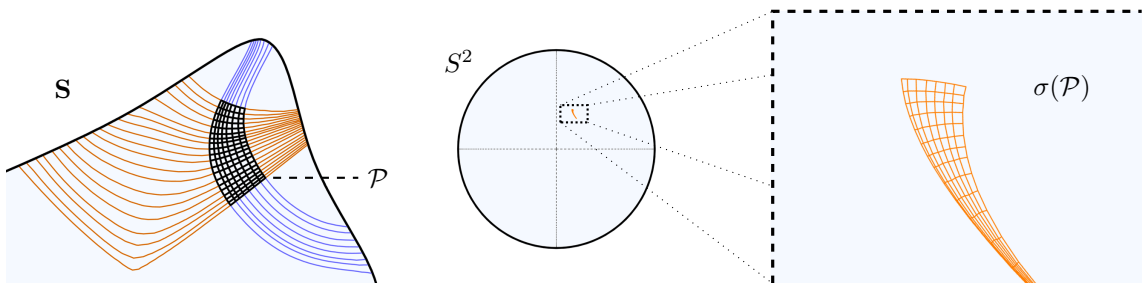


**Figure 10:** We consider a nearly developable patch of a surface  $S$  and the two families of principal curvature lines of  $S$  (blue and orange lines) over that patch. These families define a principal net denoted with  $\mathcal{P}$ . The Gauss image  $\sigma(\mathcal{P})$  of the net is displayed on the right.

number of...			weights			final energies			number of iterations	time [sec]		
ctrl.pts	patches	variables	$w_d$	$w_c$	$w_f$	$E_d$	$E_c$	$E_f$		$T_{\text{total}}$	$T_{\text{solver}}$	$T_{\text{iter}}$
91	200	1073	100	0.01	0.1	2.54	1.8	0.74	60	121.76	0.13	2.03

**Table 1:** We present the detailed information for the optimization of the leather surface  $\mathbf{S}$ . The number of control points of  $\mathbf{S}$  and the number of overlapping patches that cover the surface generate the number of variables (3 per control point and 4 per patch-associated plane). The surface was evaluated at 1800 points and each patch contained 25 points. The weights were chosen to favor the developability property. The initial and intermediate total energies of the problem were  $E_0 = 9328.17$ ,  $E_5 = 2103.75$ ,  $E_{15} = 356.702$  while the order of the final total energy  $E_{60} = 5.08$  was achieved at iteration 26, where  $E_{26} = 5.38$ . Also provided, the total time, time used by the Newton solver, and the time per iteration. (measured on an Intel® Core™ i7-6700HQ processor.

**Example 5.2.** In this example, we will focus on optimizing two relatively simple non-developable surfaces for planarity of their respective Gauss images. We start with two bicubic Bézier surfaces  $\mathbf{S}_0^a$  and  $\mathbf{S}_0^b$ , where  $\mathbf{S}_0^a$  is of mainly negative Gaussian curvature and  $\mathbf{S}_0^b$  of positive Gaussian curvature.

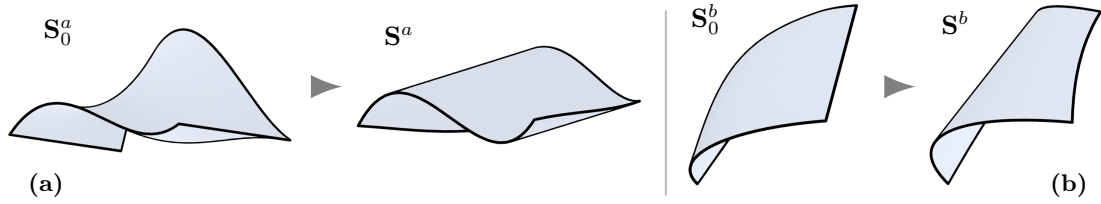


**Figure 11:** The initial surfaces  $\mathbf{S}_0^a$ ,  $\mathbf{S}_0^b$  and the optimized surfaces  $\mathbf{S}^a$ ,  $\mathbf{S}^b$  are shown from an appropriate angle to better showcase the emergence of rulings in the direction of least absolute principal curvature on each of the surfaces.

We follow optimization problem 3, defined over a single panel, and utilize only the closeness and developability terms. Given that the surfaces have approximately planar Gauss images after the optimization, we also execute the following procedure at a point set  $U$  on the surface to extrapolate the approximate rulings that are derived from their planar Gauss images, defined by the target plane  $H$ . We do this to present a visual comparison between these induced rulings and the computed rulings on the optimized surface.

---

#### Procedure Induced rulings

---

```

for all  $\mathbf{p} \in U$  do
     $\mathbf{n} \leftarrow \sigma(\mathbf{p})$ 
     $\mathbf{q} \leftarrow \text{closest point of } \mathbf{n} \text{ to target circle } H \cap S^2$ 
     $\mathbf{r}_q^t \leftarrow \text{vector tangent to target circle at } \mathbf{q}$ 
     $\mathbf{r}_q^o \leftarrow \text{vector tangent to } S^2 \text{ at } \mathbf{q} \text{ and orthogonal to } \mathbf{r}_q^t$ 
     $\text{translate vectors } \mathbf{r}_q^t, \mathbf{r}_q^o \text{ to } \mathbf{p}$  ▷ induced ruling direction
end for

```

---

The vector  $\mathbf{r}_q^o$  approximates the direction of the line generator of the surface at point  $\mathbf{q}$ . Moreover, for non-inflection rulings and non-planar regions on the optimized surfaces, vectors  $\mathbf{r}_q^t$ ,  $\mathbf{r}_q^o$  correspond to the principal directions of the surface at point  $\mathbf{q}$ .

Figure 11 shows the surfaces before and after the optimization, as well as the resulting vectors from the *Induced rulings* procedure.

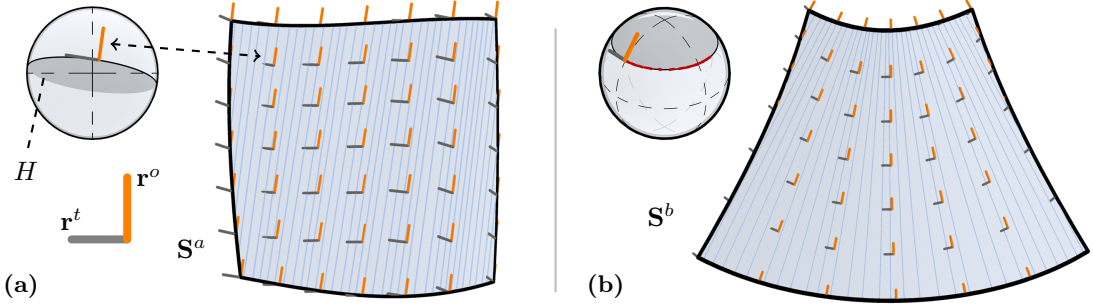


**Figure 12:** A top-down perspective of the optimized surfaces  $\mathbf{S}^a$ ,  $\mathbf{S}^b$  is shown with the rulings superimposed on the surfaces (darker blue lines) as well as the resulting vectors from the predefined *Induced rulings* procedure. We draw attention to the comparison between the orthogonal vectors  $\mathbf{r}^o$  (orange) and the direction of the rulings (vanishing principal curvature direction). Furthermore, vectors  $\mathbf{r}^t$  correspond to the directions of nonzero principal direction.

Fig. No.	number of...				weights $w_d$	final energies $E_d$	number of iterations	time [sec]		
	ctrl.pts	panels	variables	eval.pts				$w_c$	$E_c$	$T_{\text{total}}$
11a	16	1	52	169	100	0.65	10	1	81.28	1.9
11b	16	1	52	169	100	1.45	10	1	99.21	2.05

**Table 2:** The statistics for the Gauss image planarity optimization of panel surfaces  $\mathbf{S}_0^a$  and  $\mathbf{S}_0^b$ . The weights were chosen to favor the developability property. The experiment was performed on an Intel® Core™ i7-6700HQ processor.

**Example 5.3.** We provide here an introductory example of paneling a simple double curved surface with a variable number of rotational cylindrical panels.

We consider a surface  $\mathbf{S}_{\text{ref}}$  which is a subset of the positive-Gaussian-curvature part of a torus. The active surface  $\mathbf{S}$  of the optimization consists of a  $N \times 1$  grid of bicubic panels. The initial configuration of  $\mathbf{S}$  is given by fitting surface  $\mathbf{S}$  to  $\mathbf{S}_{\text{ref}}$ .

We optimize for the panels of  $\mathbf{S}$  to be rotational cylinders in the following manner. First of all, we use Lemma 4.1 and assign to each panel an energy term of the form (8) with  $d_r = 0$  since we are interested in only cylindrical panels. We then solve optimization problem 3 with equal weights assigned to  $E_d$  and  $E_r$ , and relatively smaller weights assigned to  $E_c$  and  $E_f$ .

Figure 13 shows the resulting panelization for different values of  $N$ . We wish to direct the reader's focus to the curved boundary lines that follow the reference design; a characteristic not present and inherently not possible without trimming in previous approaches that utilized strips linear in one direction.

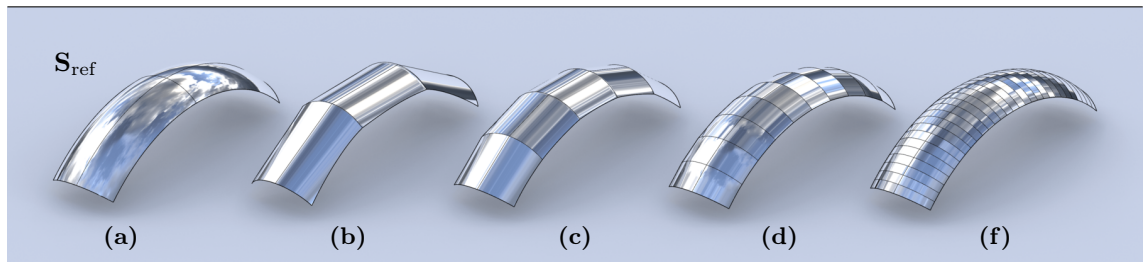


**Figure 13:** Paneling part of a torus with a different number of cylindrical panels. Both the cutting planes  $U_r$  per panel  $\mathbf{S}^{(r)}$  and the inner boundary curves follow the direction of the smaller radius circles that define the torus.

Fig. No.	number of...			weights				final energies			number of iterations	time [sec]		
	ctrl.pts	panels	variables	$w_d$	$w_r$	$w_c$	$w_f$	$E_{d+r}^\dagger$	$E_c$	$E_f$		$T_{total}$	$T_{solver}$	$T_{iter}$
13b	40	3	132	$10^2$	1	1	0.1	0.043	9.97	5.05	5	1.12	0.02	0.22
13c	64	5	212	$10^2$	1	1	0.1	0.004	2.09	5.01	5	2.05	0.03	0.4
13d	124	10	412	$10^3$	10	1	0.1	0.003	0.26	7.11	5	2.99	0.05	0.6
13e	364	30	1212	$10^3$	10	1	0.1	0.0002	0.05	18.68	5	8.11	0.17	1.62

$$^\dagger E_{d+r} = E_d + E_r$$

**Table 3:** The statistics for the paneling of the torus subsurface  $\mathbf{S}_{ref}$  for different numbers of panels. Each panel was sampled uniformly at  $4 \times 4$  points for the developability term and at  $10 \times 10$  points for the closeness term. The weights were chosen to favor the developability property. The experiment was performed on an Intel® Core™ i7-6700HQ processor.

**Example 5.4.** We extend the previous example of optimizing a simple row of panels to be of cylindrical type to the task of optimizing a grid of panels to be of any developable type we have previously addressed for panels.

Motivated by the possible architectural applications of the algorithm presented in this paper, we use as a reference surfac an architectural surface recently realized as the roof of the Department of Islamic Art at Musée du Louvre in Paris, France, shown in Figure 14. The underlying surface is a highly non-developable surface with a strong variation in the sign of Gaussian curvature. In this example, we set forth to compute an alternative realization of the same surface by using rotational conical and rotational cylindrical panels.



**Figure 14:** Detail from the *Cour Visconti* roof of the Department of Islamic Art at Musée du Louvre in Paris, France.

The user input in this case is the freeform reference surface  $\mathbf{S}_{ref}$ , the desired number of panels in each direction of the grid that will constitute the panelization of the surface and the preferred type of panels, which includes surfaces of constant slope or the more specialized and more widely-used rotational surfaces of constant slope, i.e. rotational conical and rotational cylindrical. The user by adjusting the weights of the different energy terms involved in the corresponding optimization problem 3, has influence over the various desirable aspects of the resulting panelization. In this particular example, we wish to use any of the types introduced before, namely rotational conical, rotational cylindrical and planar panels.

We present in Figure 15 the resulting panelization of the reference surface for different panel grid resolutions. We set weight  $w_c$ , corresponding to the closeness of  $\mathbf{S}$  to  $\mathbf{S}_{ref}$ , relatively high to reinforce the resulting surface to not deviate significantly from the reference surface and closely follow the chosen design. The smoothness of the boundary curves is controlled by the fairness energy term weight  $w_f$ , which is assigned a small value to ensure more visually pleasing results.

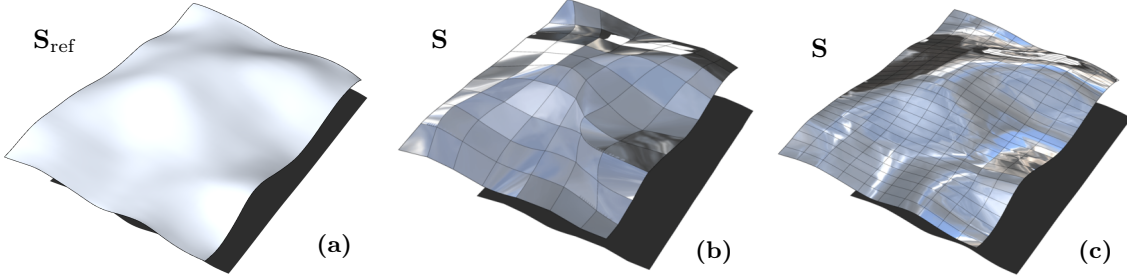


**Figure 15:** (a) The freeform reference surface to be panelized. (b) A coarse panelization consisting of 70 panels. (c) A denser panelization consisting of 300 panels. Runtime for both the coarse and the finer paneling was several minutes.

The coarse panelization of Figure 15b serves as a nice example of the dynamic panel layout adaptability which aims to approximate the given reference surface while satisfying the developability, rotationality and closeness constraints. On the contrary, by increasing the number of the panels utilized, we achieve the dense panelization of Figure 15c. As expected the increased number of panels produces an improved result, compared to the coarse equivalent. It not only better approximates the reference surface but also satisfies to a higher degree the additional secondary constraints, yielding a panelization of the reference surface that allows for a more structured arrangement of the panels.

Nevertheless, both results are welcome since each one of them serves as a valid panelization with specialized developables of the same architectural surface. Each one manages to be architecturally aesthetically pleasing in its own style, while being realizable only by rotational cylindrical and rotational conical panels; highlighting the freedom of design expression that this method provides.

**Limitations.** Among the limitations of our research, we first point to the lack of a material-dependent measure for the deviation from developability. The thickness of the Gauss image alone is not sufficient for judging whether a panel, fabricated from hardly stretchable material, can be easily bent into the computed shape. Moreover, our current implementation for paneling is limited to a grid type arrangement of panels and could benefit from additional improvements to the optimizer.

**Conclusion.** We have introduced a methodology for increasing the developability of surfaces through an optimization algorithm which aims at a thin Gauss image. Our implementation uses B-spline surfaces, but an analogous approach could be formulated for other surface representations as well. Moreover, we have presented a novel paneling algorithm which—in contrast to prior work [25]—optimizes both for the panels and the curve network of panel boundaries, under the constraint that panels are developable with a planar Gauss image and/or rotational.

**Future work.** A promising and important direction for future work is to incorporate a specific material behavior. For example, it would be nice to come up with an efficient algorithm that automatically enforces the design of only those surfaces which can easily be produced from a given material. In particular, materials which bend much more easily than they stretch are of high interest. This leads into the geometrically largely unexplored area of nearly developable surfaces. The paneling algorithm would greatly benefit from an extension to more general panel arrangements, maybe incorporating user interaction supported by automatic suggestions of the system.

## 6. Acknowledgements

We would like to thank Heinz Schmiedhofer for providing the scan and picture of the leather surface example in Figure 6. This project has received funding from the European Union’s Horizon 2020 research and innovation programme under the Marie Skłodowska-Curie grant agreement No 675789.

## References

[1] J. Lang, O. Röschel, Developable  $(1, n)$ -Bézier surfaces, Computer Aided Geometric Design 9 (4) (1992) 291 – 298. [doi:10.1016/0167-8396\(92\)90036-0](https://doi.org/10.1016/0167-8396(92)90036-0).

[2] G. Aumann, Interpolation with developable Bézier patches, *Computer Aided Geometric Design* 8 (5) (1991) 409 – 420. [doi:10.1016/0167-8396\(91\)90014-3](https://doi.org/10.1016/0167-8396(91)90014-3).

[3] G. Aumann, A simple algorithm for designing developable Bézier surfaces, *Computer Aided Geometric Design* 20 (8-9) (2003) 601–619. [doi:10.1016/j.cagd.2003.07.001](https://doi.org/10.1016/j.cagd.2003.07.001).

[4] C.-H. Chu, C. Séquin, Developable Bézier patches: properties and design, *Computer-Aided Design* 34 (7) (2002) 511 – 527. [doi:10.1016/S0010-4485\(01\)00122-1](https://doi.org/10.1016/S0010-4485(01)00122-1).

[5] C.-H. Chu, J.-T. Chen, Geometric design of uniform developable B-spline surfaces, in: International Design Engineering Technical Conferences and Computers and Information in Engineering Conference, Vol. 1: 30th Design Automation Conference, 2004, pp. 431–436. [doi:10.1115/DETC2004-57257](https://doi.org/10.1115/DETC2004-57257).

[6] H. Pottmann, J. Wallner, *Computational Line Geometry*, Springer, 2001. [doi:10.1007/978-3-642-04018-4](https://doi.org/10.1007/978-3-642-04018-4).

[7] C. Tang, P. Bo, J. Wallner, H. Pottmann, Interactive design of developable surfaces, *ACM Transactions on Graphics* 35 (2) (2016) 12:1–12:12. [doi:10.1145/2832906](https://doi.org/10.1145/2832906).

[8] W. Frey, Modeling buckled developable surfaces by triangulation, *Computer-Aided Design* 36 (4) (2004) 299 – 313. [doi:10.1016/S0010-4485\(03\)00105-2](https://doi.org/10.1016/S0010-4485(03)00105-2).

[9] J. Mitani, H. Suzuki, Making papercraft toys from meshes using strip approximate unfolding, *ACM Transactions on Graphics* 23 (3) (2004) 259–263, Proc. SIGGRAPH. [doi:10.1145/1015706.1015711](https://doi.org/10.1145/1015706.1015711).

[10] K. Rose, A. Sheffer, J. Wither, M.-P. Cani, B. Thibert, Developable surfaces from arbitrary sketched boundaries, in: Proceedings of the Fifth Eurographics Symposium on Geometry Processing, SGP '07, Eurographics Association, 2007, pp. 163–172.

[11] C. Wang, K. Tang, Achieving developability of a polygonal surface by minimum deformation: a study of global and local optimization approaches, *The Visual Computer* 20 (8) (2004) 521–539. [doi:10.1007/s00371-004-0256-0](https://doi.org/10.1007/s00371-004-0256-0).

[12] A. Jung, S. Hahmann, D. Rohmer, A. Begault, L. Boissieux, M.-P. Cani, Sketching folds: Developable surfaces from non-planar silhouettes, *ACM Trans. Graph.* 34 (5) (2015) 155:1–155:12. [doi:10.1145/2749458](https://doi.org/10.1145/2749458).

[13] P. Decaudin, D. Julius, J. Wither, L. Boissieux, A. Sheffer, M.-P. Cani, Virtual garments: A fully geometric approach for clothing design, *Computer Graphics Forum* 25 (3) (2006) 625–634. [doi:10.1111/j.1467-8659.2006.00982.x](https://doi.org/10.1111/j.1467-8659.2006.00982.x).

[14] Y. Liu, H. Pottmann, J. Wallner, Y.-L. Yang, W. Wang, Geometric modeling with conical meshes and developable surfaces, *ACM Transactions on Graphics* 25 (3) (2006) 681–689. [doi:10.1145/1141911.1141941](https://doi.org/10.1145/1141911.1141941).

[15] J. Solomon, E. Vouga, M. Wardetzky, E. Grinspun, Flexible developable surfaces, *Computer Graphics Forum* 31 (5) (2012) 1567–1576, proc. Symposium Geometry Processing. [doi:10.1111/j.1467-8659.2012.03162.x](https://doi.org/10.1111/j.1467-8659.2012.03162.x).

[16] M. Rabinovich, T. Hoffmann, O. Sorkine-Hornung, Discrete geodesic nets for modeling developable surfaces, *ACM Transactions on Graphics* 37 (2) (2018) 16:1–16:17. [doi:10.1145/3180494](https://doi.org/10.1145/3180494).

[17] F. Pérez, J. A. Suárez, Quasi-developable B-spline surfaces in ship hull design, *Computer-Aided Design* 39 (10) (2007) 853 – 862. [doi:10.1016/j.cad.2007.04.004](https://doi.org/10.1016/j.cad.2007.04.004).

[18] M. Chen, K. Tang, A fully geometric approach for developable cloth deformation simulation, *The Visual Computer* 26 (6) (2010) 853–863. [doi:10.1007/s00371-010-0467-5](https://doi.org/10.1007/s00371-010-0467-5).

[19] D. Julius, V. Kraevoy, A. Sheffer, D-charts: Quasi-developable mesh segmentation, *Computer Graphics Forum* 24 (3) (2005) 581–590, Proc. of Eurographics. [doi:10.1111/j.1467-8659.2005.00883.x](https://doi.org/10.1111/j.1467-8659.2005.00883.x).

[20] H. Yamauchi, S. Gumhold, R. Zayer, H.-P. Seidel, Mesh segmentation driven by Gaussian curvature, *The Visual Computer* 21 (8) (2005) 659–668. [doi:10.1007/s00371-005-0319-x](https://doi.org/10.1007/s00371-005-0319-x).

[21] R. Narain, T. Pfaff, J. F. O’Brien, Folding and crumpling adaptive sheets, *ACM Transactions on Graphics* 32 (4) (2013) 51:1–51:8, Proc. SIGGRAPH. [doi:10.1145/2461912.2462010](https://doi.org/10.1145/2461912.2462010).

[22] C. C. L. Wang, Y. Wang, M. M.-F. Yuen, On increasing the developability of a trimmed NURBS surface, *Engineering with Computers* 20 (1) (2004) 54–64. [doi:10.1007/s00366-004-0272-8](https://doi.org/10.1007/s00366-004-0272-8).

[23] O. Stein, E. Grinspun, K. Crane, Developability of triangle meshes, *ACM Transactions on Graphics* 37 (4), Proc. SIGGRAPH.

[24] H. Pottmann, M. Eigensatz, A. Vaxman, J. Wallner, Architectural geometry, *Computers and Graphics* 47 (2015) 145–164. [doi:<http://dx.doi.org/10.1016/j.cag.2014.11.002>](http://dx.doi.org/10.1016/j.cag.2014.11.002).

[25] M. Eigensatz, M. Kilian, A. Schiftner, N. Mitra, H. Pottmann, M. Pauly, Paneling architectural freeform surfaces, *ACM Transactions on Graphics* 29 (4) (2010) 45:1–45:10, Proc. SIGGRAPH. [doi:10.1145/1778765.1778782](https://doi.org/10.1145/1778765.1778782).

[26] H. Pottmann, A. Schiftner, P. Bo, H. Schmiedhofer, W. Wang, N. Baldassini, J. Wallner, Freeform surfaces from single curved panels, *ACM Transactions on Graphics* 27 (3) (2008) 76:1–76:10, Proc. SIGGRAPH. [doi:10.1145/1360612.1360675](https://doi.org/10.1145/1360612.1360675).

[27] A. Schiftner, M. Eigensatz, M. Kilian, G. Chinzi, Large scale double curved glass facades made feasible – the Arena Corinthians west facade, in: *Glass Performance Days Finland (Conference Proceedings)*, 2013, pp. 494 – 498.

[28] D. Shelden, Digital surface representation and the constructibility of Gehry’s architecture, Ph.D. thesis, M.I.T. (2002).

[29] M. Schneider, P. Mehrtens, Cladding freeform surfaces with curved metal panels – a complete digital production chain, in: *Advances in Architectural Geometry 2012*, Springer, 2013, pp. 237–242. [doi:10.1007/978-3-7091-1251-9\\_19](https://doi.org/10.1007/978-3-7091-1251-9_19).

[30] R. Farouki, *Pythagorean-Hodograph Curves: Algebra and Geometry Inseparable*, Springer, 2008. [doi:10.1007/978-3-540-73398-0](https://doi.org/10.1007/978-3-540-73398-0).

[31] A. Vavpetič, E. Žagar, A general framework for the optimal approximation of circular arcs by parametric polynomial curves, *Journal of Computational and Applied Mathematics* 345 (2019) 146 – 158. [doi:10.1016/j.cam.2018.06.020](https://doi.org/10.1016/j.cam.2018.06.020).

[32] T. W. Dubé, The structure of polynomial ideals and Gröbner bases, *SIAM Journal on Computing* 19 (4) (1990) 750–773. [doi:10.1137/0219053](https://doi.org/10.1137/0219053).

[33] L. Piegl, W. Tiller, *The NURBS Book*, 2nd Edition, Springer, 1997. [doi:10.1007/978-3-642-59223-2](https://doi.org/10.1007/978-3-642-59223-2).

[34] H. Pottmann, S. Leopoldseder, M. Hofer, Registration without ICP, *Computer Vision and Image Understanding* 95 (1) (2004) 54–71. [doi:10.1016/j.cviu.2004.04.002](https://doi.org/10.1016/j.cviu.2004.04.002).

[35] W. Wang, H. Pottmann, Y. Liu, Fitting B-spline curves to point clouds by curvature-based squared distance minimization, *ACM Transactions on Graphics* 25 (2) (2006) 214–238. [doi:10.1145/1138450.1138453](https://doi.org/10.1145/1138450.1138453).

[36] J. Nocedal, S. Wright, *Numerical Optimization*, Springer Series in Operations Research and Financial Engineering, Springer, 2006. [doi:10.1007/978-0-387-40065-5](https://doi.org/10.1007/978-0-387-40065-5).

[37] Y. Liu, H. Pottmann, W. Wang, Constrained 3D shape reconstruction using a combination of surface fitting and registration, *Computer-Aided Design* 38 (6) (2006) 572 – 583. [doi:<https://doi.org/10.1016/j.cad.2006.01.014>](https://doi.org/10.1016/j.cad.2006.01.014).

[38] H. Pottmann, T. Randrup, Rotational and helical surface approximation for reverse engineering, *Computing* 60 (4) (1998) 307–322. [doi:10.1007/BF02684378](https://doi.org/10.1007/BF02684378).